

Draft Genome Sequence of the Sexually Transmitted Pathogen *Trichomonas vaginalis*

Jane M. Carlton,^{1*} Robert P. Hirt,² Joana C. Silva,¹ Arthur L. Delcher,³ Michael Schatz,³ Qi Zhao,¹ Jennifer R. Wortman,¹ Shelby L. Bidwell,¹ U. Cecilia M. Alsmark,² Sébastien Besteiro,⁴ Thomas Sicheritz-Ponten,⁵ Christophe J. Noel,² Joel B. Dacks,⁶ Peter G. Foster,⁷ Cedric Simillion,⁸ Yves Van de Peer,⁸ Diego Miranda-Saavedra,⁹ Geoffrey J. Barton,⁹ Gareth D. Westrop,⁴ Sylke Müller,⁴ Daniele Dessi,¹⁰ Pier Luigi Fiori,¹⁰ Qinghu Ren,¹ Ian Paulsen,¹ Hanbang Zhang,¹ Felix D. Bastida-Corcuera,¹¹ Augusto Simoes-Barbosa,¹¹ Mark T. Brown,¹¹ Richard D. Hayes,¹¹ Mandira Mukherjee,¹¹ Cheryl Y. Okumura,¹¹ Rachel Schneider,¹¹ Alias J. Smith,¹¹ Stepanka Vanacova,¹¹ Maria Villalvazo,¹¹ Brian J. Haas,¹ Mihaela Pertea,³ Tamara V. Feldblyum,¹ Terry R. Utterback,¹² Chung-Li Shu,¹³ Kazutoyo Osoegawa,¹³ Pieter J. de Jong,¹³ Ivan Hrdy,¹⁴ Lenka Horvathova,¹⁴ Zuzana Zubacova,¹⁴ Pavel Dolezal,¹⁴ Shehre-Banoo Malik,¹⁵ John M. Logsdon Jr.,¹⁵ Katrin Henze,¹⁶ Arti Gupta,¹⁷ Ching C. Wang,¹⁷ Rebecca L. Dunne,¹⁸ Jacqueline A. Upcroft,¹⁹ Peter Upcroft,¹⁹ Owen White,¹ Steven L. Salzberg,³ Petrus Tang,²⁰ Cheng-Hsun Chiu,²¹ Ying-Shiung Lee,²² T. Martin Embley,² Graham H. Coombs,²³ Jeremy C. Mottram,⁴ Jan Tachezy,¹⁴ Claire M. Fraser-Liggett,¹ Patricia J. Johnson¹¹

We describe the genome sequence of the protist *Trichomonas vaginalis*, a sexually transmitted human pathogen. Repeats and transposable elements comprise about two-thirds of the ~160-megabase genome, reflecting a recent massive expansion of genetic material. This expansion, in conjunction with the shaping of metabolic pathways that likely transpired through lateral gene transfer from bacteria, and amplification of specific gene families implicated in pathogenesis and phagocytosis of host proteins may exemplify adaptations of the parasite during its transition to a urogenital environment. The genome sequence predicts previously unknown functions for the hydrogenosome, which support a common evolutionary origin of this unusual organelle with mitochondria.

Trichomonas vaginalis is a flagellated protist that causes trichomoniasis, a common but overlooked sexually transmitted human infection, with ~170 million cases occurring annually worldwide (1). The extracellular parasite resides in the urogenital tract of both sexes and can cause vaginitis in women and urethritis and prostatitis in men. Acute infections are associated with pelvic inflammatory disease, increased risk of human immunodeficiency virus 1 (HIV-1) infection, and adverse pregnancy outcomes. *T. vaginalis* is a member of the parabasalid lineage of microaerophilic eukaryotes that lack mitochondria and peroxisomes but contain unusual organelles called hydrogenosomes. Although previously considered to be one of the earliest branching eukaryotic lineages, recent analyses leave the evolutionary relationship of parabasalids to other major eukaryotic groups unresolved (2, 3). In this article, we report the draft sequence of *T. vaginalis*, the first parabasalid genome to be described.

Genome structure, RNA processing, and lateral gene transfer. The *T. vaginalis* genome sequence, generated using whole-genome shotgun methodology, contains 1.4 million shotgun reads assembled into 17,290 scaffolds at ~7.2× coverage (4). At least 65% of the *T. vaginalis* genome is repetitive (table S1). Despite several procedures developed to improve the assembly

(4), the superabundance of repeats resulted in a highly fragmented sequence, preventing investigation of *T. vaginalis* genome architecture. The repeat sequences also hampered measurement of genome size, but we estimate it to be ~160 Mb (4). A core set of ~60,000 protein-coding genes was identified (Table 1), endowing *T. vaginalis* with one of the highest coding capacities among eukaryotes (table S2). Introns were identified in 65 genes, including the ~20 previously documented (5). Transfer RNAs (tRNAs) for all 20 amino acids were found, and ~250 ribosomal DNA (rDNA) units were identified on small contigs and localized to one of the six *T. vaginalis* chromosomes (Fig. 1).

The Inr promoter element was found in ~75% of 5' untranslated region (UTR) sequences (4), supporting its central role in gene expression (6). Intriguingly, the eukaryotic transcription machinery of *T. vaginalis* appears more metazoan than protistan (table S3 to S5). The presence of a *T. vaginalis* Dicer-like gene, two Argonaute genes, and 41 transcriptionally active DEAD-DEAH-box helicase genes suggests the existence of an RNA interference (RNAi) pathway (fig. S1). Identification of these components raises the possibility of using RNAi technology to manipulate *T. vaginalis* gene expression.

During genome annotation, we identified 152 cases of possible prokaryote-to-eukaryote lateral

gene transfer (LGT) [tables S6 and S7 and Supporting Online Material (SOM) text], augmenting previous reports of conflicting phylogenetic relationships among several enzymes (7). The putative functions of these genes are diverse, affecting various metabolic pathways (fig. S2) and strongly influencing the evolution of the *T. vaginalis* metabolome. A majority (65%) of the 152 LGT genes encode metabolic enzymes, more than a third of which are involved in carbohydrate or amino acid metabolism (Fig. 2). Several LGT genes may have been acquired from Bacteroidetes-related bacteria, which are abundant among vertebrate intestinal flora (fig. S3).

Repeats, transposable elements, and genome expansion. The most common 59 repeat families identified in the assembly (4) constitute ~39 Mb of the genome and can be classified as (i) virus-like; (ii) transposon-like, including ~1000 copies of the first *mariner* element identified outside animals (8); (iii) retrotransposon-like; and (iv) unclassified (Table 2). Most of the

¹Institute for Genomic Research, 9712 Medical Research Drive, Rockville, MD 20850, USA. ²Division of Biology, Devonshire Building, Newcastle University, Newcastle upon Tyne NE1 7RU, UK. ³Center for Bioinformatics and Computational Biology, University of Maryland, College Park, MD 20742, USA. ⁴Wellcome Centre for Molecular Parasitology and Division of Infection and Immunity, Glasgow Biomedical Research Centre, University of Glasgow, Glasgow G12 8TA, UK. ⁵Center for Biological Sequence Analysis, Biocentrum-DTU, Technical University of Denmark, DK-2800 Lyngby, Denmark. ⁶Department of Biological Sciences, University of Calgary, 2500 University Drive NW, Calgary, Alberta T2N 1N4, Canada. ⁷Department of Zoology, Natural History Museum, Cromwell Road, London SW7 5BD, UK. ⁸Department of Plant Systems Biology, Flanders Interuniversity Institute for Biotechnology (VIB), Ghent University, Technologiepark 927, B-9052 Ghent, Belgium. ⁹School of Life Sciences Research, University of Dundee, Dow Street, Dundee DD1 5EH, UK. ¹⁰Department of Biomedical Sciences, Division of Experimental and Clinical Microbiology, University of Sassari, Viale San Pietro 43/b, 07100 Sassari, Italy. ¹¹Department of Microbiology, Immunology, and Molecular Genetics, University of California, Los Angeles, CA 90095-1489, USA. ¹²J. Craig Venter Joint Technology Center, 5 Research Place, Rockville, MD 20850, USA. ¹³Children's Hospital Oakland Research Institute, 747 52nd Street, Oakland, CA 94609, USA. ¹⁴Department of Parasitology, Faculty of Science, Charles University, 128 44 Prague, Czech Republic. ¹⁵Department of Biological Sciences, Roy J. Carver Center for Comparative Genomics, University of Iowa, Iowa City, IA 52242-1324, USA. ¹⁶Institute of Botany, Heinrich Heine University, 40225 Düsseldorf, Germany. ¹⁷Department of Pharmaceutical Chemistry, University of California, San Francisco, CA 94143-2280, USA. ¹⁸Department of Microbiology and Parasitology, University of Queensland, Brisbane, Queensland 4072, Australia. ¹⁹Queensland Institute of Medical Research, Brisbane, Queensland 4029, Australia. ²⁰Bioinformatics Center/Molecular Medicine Research Center, Chang Gung University, Taoyuan 333, Taiwan. ²¹Molecular Infectious Diseases Research Center, Chang Gung Memorial Hospital, Taoyuan 333, Taiwan. ²²Medical Genomic Center, Chang Gung Memorial Hospital, Taoyuan 333, Taiwan. ²³Strathclyde Institute of Pharmacy and Biomedical Sciences, John Arbuthnot Building, University of Strathclyde, Glasgow G4 0NR, UK.

*To whom correspondence should be addressed. E-mail: jane.carlton@med.nyu.edu

†Present address: Department of Medical Parasitology, New York University School of Medicine, New York, NY 10011, USA.

59 repeats are present in hundreds of copies (average copy number ~660) located on small (1- to 5-kb) contigs, and each repeat family is extraordinarily homogenous, with an average polymorphism of ~2.5%.

The lack of a strong correlation between copy number and average pairwise difference between copies (fig. S4) suggests that a sudden expansion of the repeat families had occurred. To estimate the time of expansion, we compared the degree of polymorphism among *T. vaginalis* repeats to

Table 1. Summary of the *T. vaginalis* genome sequence data. Assembly size (bp, base pairs) includes all contigs and differs from estimated genome size of ~160 Mb (4). The scaffold size is the minimum scaffold length, such that more than half the genome is contained in scaffolds of at least that length. The number of predicted genes may include low-complexity repeats or novel transposable elements rather than true *T. vaginalis* genes, but in the absence of decisive evidence these remain in the gene set. The number of evidence-supported genes includes those with either similarity to a known protein ($E < 1 \times 10^{-10}$, >25% length of protein) or similarity to an expressed sequence tag (>95% identity over >90% length of the gene). A total of 763 rDNA fragments (258 copies of 28S, 254 copies of 18S, and 251 copies of 5.8S) were identified.

Feature	Value
<i>Genome</i>	
Size of assembly (bp)	176,441,227
G+C content (%)	32.7
No. of scaffolds	17,290
N_{50} scaffold size (bp)	68,338
<i>Protein-coding genes</i>	
No. of predicted genes	59,681
No. of evidence-supported genes	25,949
No. of genes with introns	65
Mean gene length (bp)	928.6
Gene G+C content (%)	35.5
Gene density (bp)	2956
Mean length of intergenic regions (bp)	1165.4
Intergenic G+C content (%)	28.8
<i>Non-protein-coding genes</i>	
Predicted tRNA genes	479
Predicted 5.8S, 18S, and 28S rDNA units	~250

the divergence between *T. vaginalis* and its sister taxon *T. tenax*, a trichomonad of the oral cavity (9), for several protein-coding loci (4). Our results indicate that repeat family amplification occurred after the two species split (table S8). Several families have also undergone multiple expansions, as implied by bi- or trimodal distribution of pairwise distances between copies (fig. S5). *T. vaginalis* repeat families appear to be absent in *T. tenax* but are present in geographically diverse *T. vaginalis* (4), consistent with the expansion having occurred after speciation but before diversification of *T. vaginalis*.

The large genome size, high repeat copy number, low repeat polymorphism, and evidence of repeat expansion after *T. vaginalis* and *T. tenax* diverged suggest that *T. vaginalis* has undergone a very recent and substantial increase in genome size. To determine whether the genome underwent any large-scale duplication event(s), we analyzed age distributions of gene families with five or fewer members (4). A peak in the age distribution histogram of pairs of gene families was observed (fig. S6), indicating that the genome underwent a period of increased duplication, and possibly one or more large-scale genome duplication events.

Metabolism, oxidative stress, and transport. *T. vaginalis* uses carbohydrate as a main energy source via fermentative metabolism under aerobic and anaerobic conditions. We found the parasite to use a variety of amino acids as energy substrates (Fig. 2) (10), with arginine dihydrolase metabolism a major pathway for energy production (fig. S7) (11). We confirmed a central role for aminotransferases (Fig. 2 and table S9) and glutamate dehydrogenase as indicated previously (12, 13); these pathways are likely catabolic but may be reversible to allow the parasite to synthesize glutamate, aspartate, alanine, glutamine, and glycine. Genes required for synthesis of proline from arginine (fig. S7) and for threonine metabolism (fig. S8) were identified. We also identified a de novo biosynthesis pathway for cysteine via cysteine synthase, an LGT candidate (fig. S8) (14), and genes encoding enzymes involved in methionine metabolism, including its possible regeneration (fig. S9).

Earlier studies indicated that de novo lipid biosynthesis in *T. vaginalis* is confined to the major phospholipid phosphatidylethanolamine

(PE) (15), whereas other lipids, including cholesterol, are likely acquired from exogenous sources. We found an absence of several essential enzyme-encoding genes in the synthesis and degradation pathways of nearly all lipids (4), in contrast to the PE synthetic pathway, which appears complete; however, experimental verification of these results is required.

T. vaginalis is microaerophilic with a primarily anaerobic life style and thus requires redox and antioxidant systems to counter the detrimental effects of oxygen. Genes encoding a range of defense molecules, such as superoxide dismutases, thioredoxin reductases, peroxiredoxins, and rubrerythrins, were identified (table S10).

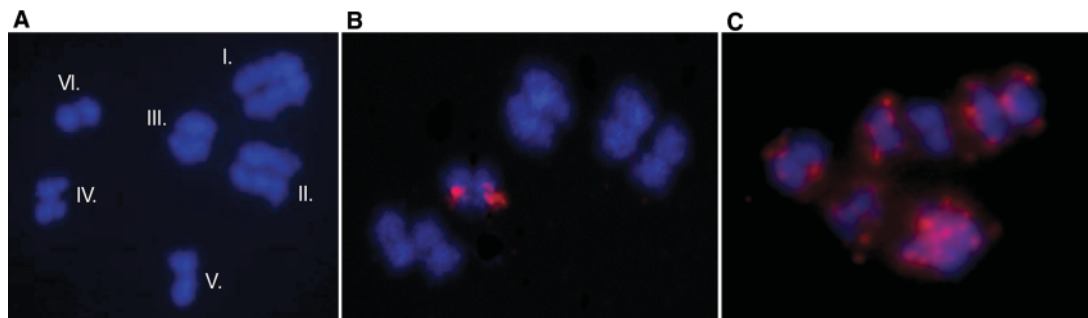
T. vaginalis demonstrates a broad range of transport capabilities, facilitated by expansion of particular transporter families, such as those for sugar and amino acids (table S11). The parasite also possesses more members of the cation-chloride cotransporter (CCC) family than any other sequenced eukaryote, likely reflecting osmotic changes faced by the parasite in a mucosal environment.

None of the proteins required for glycosylphosphatidylinositol (GPI)-anchor synthesis were identified in the genome sequence, making *T. vaginalis* the first eukaryote known to lack an apparent GPI-anchor biosynthetic pathway. Whether *T. vaginalis* has evolved an unusual biosynthetic pathway for synthesis of its nonprotein lipid anchors, such as the inositol-phosphoceramide of surface lipophosphoglycans (16), remains to be determined.

Massively expanded gene families. Many gene families in the *T. vaginalis* genome have undergone expansion on a scale unprecedented in unicellular eukaryotes (Table 3). Such “conservative” gene family expansions are likely to improve an organism’s adaptation to its environment (17). Notably, the selective expansion of subsets of the membrane trafficking machinery, critical for secretion of pathogenic proteins, endocytosis of host proteins, and phagocytosis of bacteria and host cells (table S12), correlates well with the parasite’s active endocytic and phagocytic life-style.

Massively amplified gene families also occur in the parasite’s kinome, which comprises ~880 genes (SOM text) encoding distinct eukaryotic protein kinases (ePKs) and ~40 atypical protein

Fig. 1. Karyotype and fluorescent in situ hybridization (FISH) analysis of *T. vaginalis* chromosomes. (A) Metaphase chromosome squashes of *T. vaginalis* reveal six chromosomes (I to VI). (B) FISH analysis using an 18S rDNA probe shows that all ~250 rDNA units localize to a single chromosome. (C) In contrast, the *Tvmar1* transposable element (8) is dispersed throughout the genome.



kinases, making it one of the largest eukaryotic kinomes known. The parasite has heterotrimeric guanine nucleotide-binding proteins and components of the mitogen-activated protein kinase (MAPK) pathway, suggesting yeast-like signal transduction mechanisms. Unusually, the *T. vaginalis* kinome contains 124 cytosolic tyrosine kinase-like (TKL) genes, yet completely lacks receptor serine/threonine ePKs of the TKL family. Inactive kinases were found to make up 17% of the *T. vaginalis* kinome (table S13); these may act as substrates and scaffolds for assembly of signaling complexes (18). ePK accessory domains are important for regulating signaling pathways, but just nine accessory domain types were identified in 8% (72/883) of the *T. vaginalis* ePKs (table S14), whereas ~50% of human ePKs contain at least 1 of 83 accessory domain types. This suggests that regulation of protein kinase function and cell signaling in *T. vaginalis* is less complex than that in higher eukaryotes, a possible explanation for the abundance of *T. vaginalis* ePKs.

T. vaginalis possesses several unusual cytoskeletal structures: the axostyle, the pelta, and the costa (19). Most actin- and tubulin-related components of the cytoskeleton are present (table S15), with the exception of homologs of the actin motor myosin. In contrast, homologs of the microtubular motors kinesin and dynein are unusually abundant (Table 3). Thus, *T. vaginalis* intracellular transport mechanisms are mediated primarily by kinesin and cytoplasmic dynein, as described for *Dictyostelium* and filamentous fungi, raising the possibility that the loss of myosin-driven cytoplasmic transport is not uncommon in unicellular eukaryotes (20). Whether the structural remodeling of

amoeboid *T. vaginalis* during host colonization (see below) is actin-based, as described for other eukaryotes, or driven by novel cytoskeletal rearrangements remains an open question.

We identified homologs of proteins involved in DNA damage response and repair, chromatin restructuring, and meiosis, the latter a process not thought to occur in the parasite (table S16). Of the 29 core meiotic genes found, several are general repair proteins required for meiotic progression in other organisms (21), and eight are meiosis-specific proteins. Thus, *T. vaginalis* contains either recent evolutionary relics of meiotic machinery or genes functional in meiotic recombination in an as-yet undescribed sexual cycle.

Molecular mechanisms of pathogenesis.

T. vaginalis must adhere to host cells to establish and maintain an infection. A dense glycocalyx composed of lipophosphoglycan (LPG) (Fig. 3) and surface proteins has been implicated in adherence (22), but little is known about this critical pathogenic process. We identified genes encoding enzymes predicted to be required for LPG synthesis (table S17). Of particular interest are the genes required for synthesis of an unusual nucleotide sugar found in *T. vaginalis* LPG, the monosaccharide rhamnose, which is absent in the human host, making it a potential drug target. Genes (some of which are LGT candidates) were identified that are involved in sialic acid biosynthesis, consistent with the reported presence of this sugar on the parasite surface (23).

We identified eight families containing ~800 proteins (4) that represent candidate surface molecules (Fig. 3 and table S18), including ~650

highly diverse BspA-like proteins characterized by the *Treponema pallidum* leucine-rich repeat, TplLR. BspA-like proteins are expressed on the surface of certain pathogenic bacteria and mediate cell adherence and aggregation (24). The only other eukaryote known to encode BspA-like proteins, the mucosal pathogen *Entamoeba histolytica* (25), contains 91 such proteins, one of which was recently localized to the parasite surface (26).

There are >75 *T. vaginalis* GP63-like proteins, homologs of the most abundant surface proteins of *Leishmania major*, the leishmanolysins, which contribute to virulence and pathogenicity through diverse functions in both the insect vector and the mammalian host (27). Most *T. vaginalis* GP63-like genes possess the domains predicted to be required for a catalytically active metallopeptidase, including a short HEXXH motif (28) (Fig. 3). Unlike trypanosomatid GP63 proteins, which are predicted to be GPI-anchored, most *T. vaginalis* GP63-like proteins have a predicted C-terminal transmembrane domain as a putative cell surface anchor, consistent with the apparent absence of GPI-anchor biosynthetic enzymes. Other *T. vaginalis* protein families share domains with *Chlamydia* polymorphic membrane proteins, *Giardia lamblia* variant surface proteins, and *E. histolytica* immunodominant variable surface antigens (Fig. 3 and table S18).

After cytoadherence, the parasite becomes amoeboid, increasing cell-to-cell surface contacts and forming cytoplasmic projections that interdigitate with target cells (19). We have identified genes encoding cytolytic effectors, which may be released upon host-parasite contact. *T. vaginalis* lyses host red blood cells, presumably as a means of acquiring lipids and iron and possibly explaining the exacerbation of symptoms observed during menstruation (29). This hemolysis is dependent on contact, temperature, pH, and Ca^{2+} , suggesting the involvement of pore-forming proteins (30) that insert into the lipid bilayer of target cells, mediating osmotic lysis. Consistent with this, we have identified 12 genes (*TvSaplip1* to *TvSaplip12*) containing saposin-like (SAPLIP) pore-forming domains (fig. S10). These domains show a predicted six-cysteine pattern and abundant hydrophobic residues in conserved positions while displaying high sequence variability (fig. S11). The *TvSaplips* are similar to amoebapore proteins secreted by *E. histolytica* and are candidate trichopores that mediate a cytolytic effect.

The degradome. Peptidases perform many critical biological processes and are potential virulence factors, vaccine candidates, and drug targets (31). *T. vaginalis* contains an expanded degradome of more than 400 peptidases (SOM text), making it one of the most complex degradomes described (table S19). Of the three families of aspartic peptidases (table S20), *T. vaginalis* contains a single member of the HIV-1 retropepsin family that might serve as a putative candidate for anti-HIV peptidase inhibitors. Many studies have implicated papain

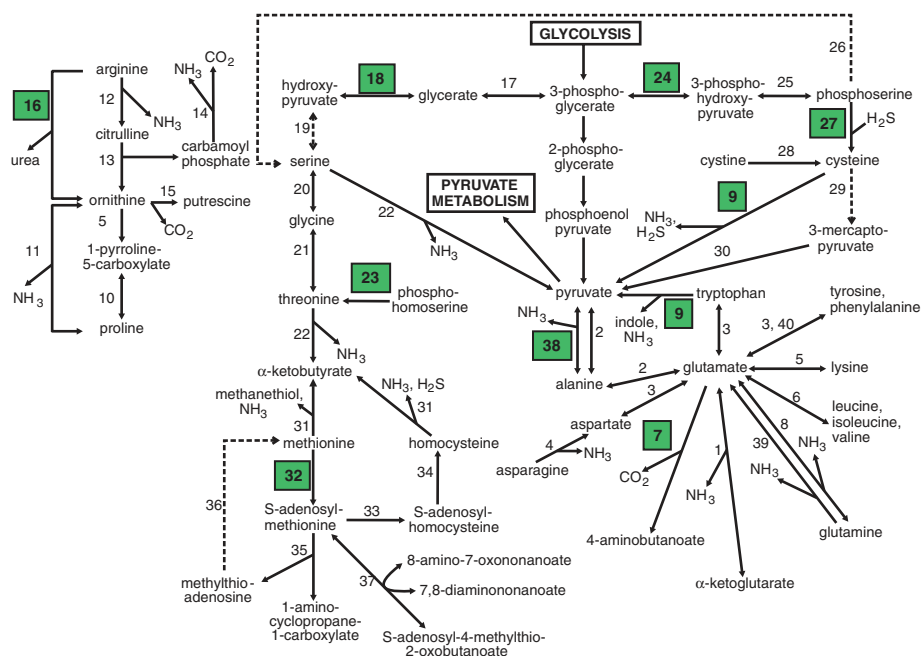


Fig. 2. Schematic of *T. vaginalis* amino acid metabolism. A complete description of enzymatic reactions (represented as numbers) is given in the SOM text. Broken lines represent enzymes for which no gene was identified in the genome sequence, although the activity would appear to be required. Green boxes indicate enzymes encoded by candidate LGT genes.

Table 2. Summary of highly repetitive sequences in the genome of *T. vaginalis*. The 31 unclassified repeat families have been collapsed into one group.

Repeat name	Putative identity	Copy no.	Length (bp)	Cumulative length (bp)	Average pairwise difference (%)
<i>Viral</i>					
R128b	Poxvirus D5 protein	203	2348	370,658	1.2
R169a	Phage tail fiber prot	903	752	607,929	3.9
R1794	Hypothetical	2243	1037	1,879,762	3.0
R299a	KilA-N terminal domain	867	873	655,984	6.6
R3a	Poxvirus D5 protein	954	2637	1,721,187	4.6
R9a	KilA-N terminal domain	831	663	503,959	3.6
R947a	KilA-N terminal domain	518	669	298,778	3.1
Average (total)		931	1283	(6,038,257)	3.7
<i>Transposon</i>					
R8	Mariner transposase	982	1304	1,158,473	0.5
R107	Integrase	384	2246	518,936	0.9
R119	Mutator-like profile	282	2954	303,256	1.1
R11b	Integrase	1842	981	1,634,764	2.1
R128a	HNH endonuclease	200	800	131,491	1.5
R130a	Mutator-like profile	173	1129	137,526	0.7
R165	Mutator-like profile	365	2410	368,152	1.1
R178	Integrase	580	2433	636,901	1.5
R204	Integrase	51	1323	51,185	1.6
R210	Mutator-like profile	75	2127	118,581	0.9
R2375	Endonuclease	566	765	329,717	5.4
R242b	Integrase	49	1151	45,564	2.5
R26b	Integrase	1148	1141	1,175,921	2.6
R289a	Integrase	54	1250	53,674	2.2
R309b	Integrase	56	1601	73,737	1.4
R414a	Integrase	37	909	27,708	1.4
R41b	Integrase	927	1184	807,711	2.5
R473	Integrase	19	1124	15,254	1.3
Integ.a95313	Integrase	68	1301	22,023	2.3
Average (total)		414	1481	(7,610,574)	1.8
<i>Retrotransposon</i>					
R1407.RT	Reverse transcriptase	6	2349	6,833	1.0
copia.a38393	Copia-like profile	7	11001	16,504	7.5
Average (total)		6.5	6675	(23,337)	4.3
<i>31 unclassified families</i>					
Average (total)		793	1131	(24,617,704)	2.6
Total all				38,289,872	
Average all		660	1450		2.5

family cysteine peptidases as virulence factors in trichomonads; we identified >40 of them, highlighting the diversity of this family. Cysteine peptidases that contribute to the 20S proteasome (ubiquitin C-terminal hydrolases) are abundant (117 members, ~25% of the degradome), emphasizing the importance of cytosolic protein degradation in the parasite. *T. vaginalis* has nine NlpC/P60-like members (table S20; several of which are LGT candidates), which play a role in bacterial cell wall degradation and the destruction of healthy vaginal microflora, making the vaginal mucosa more sensitive to other infections.

We also identified many subtilisin-like and several rhomboid-like serine peptidases, candidates for processing *T. vaginalis* surface proteins. In addition to the first asparaginase-type of threonine peptidase found in a protist, 13 families of metallopeptidases were also identi-

fied, as well as three cystatin-like proteins, natural peptidase inhibitors, which may regulate the activity of the abundant papain-like cysteine peptidases (table S20).

The hydrogenosome. Several microaerophilic protists and fungi, including trichomonads and ciliates, lack typical mitochondria and possess double-membrane hydrogenosomes, which produce adenosine triphosphate (ATP) and molecular hydrogen through fermentation of metabolic intermediates produced in the cytosol. Although the origin of these organelles has been controversial, most evidence now supports a common origin with mitochondria (3). Few genes encoding homologs of mitochondrial transporters, translocons, and soluble proteins were identified in the *T. vaginalis* genome (fig. S12), suggesting that its hydrogenosome has undergone reductive evolution comparable to other

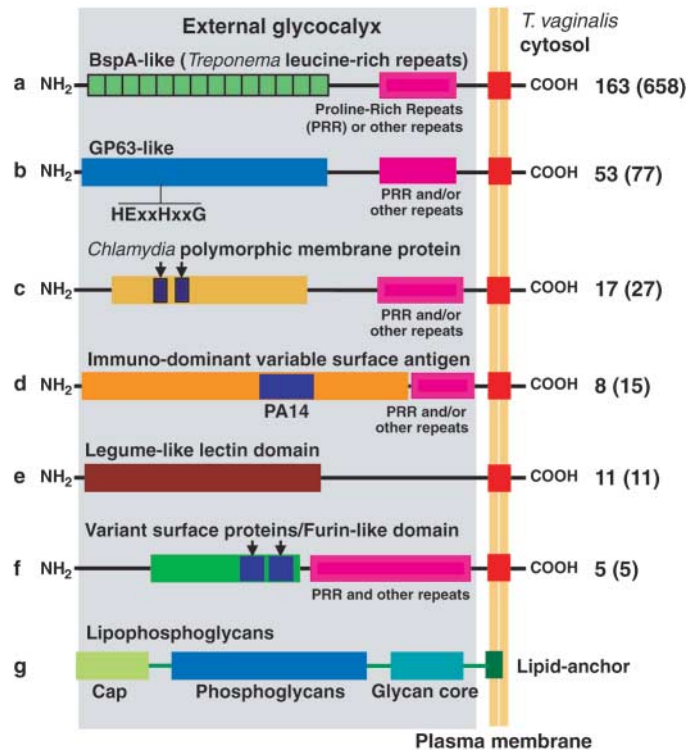
Table 3. Large gene families in *T. vaginalis*. Only gene families, or aggregates of gene families mediating a given process, for which there are more than 30 members and that have been assigned a putative function are listed. (See SOM text for subfamily organization.) The small guanosine triphosphatases (GTPases) are the sum of Rab and ARF small GTPases only; all other GTPases are shown in table S12. ABC, ATP-binding cassette; MFS, major facilitator superfamily; MOP, multi-drug/oligosaccharidyl-lipid/polysaccharide; AAAP, amino acid/auxin permease.

Gene family (functional unit)	Members
Protein kinases	927
BspA-like gene family	658
Membrane trafficking: small GTPases	328
rDNA gene cluster	~250
Cysteine peptidase (clan CA, family C19)	117
Membrane trafficking: vesicle formation	113
ABC transporter superfamily	88
GP63-like (leishmanolysin)	77
MFS transporter family	57
MOP flippase transporter family	47
Cysteine peptidase (clan CA, family C1)	48
AAAP transporter family	40
Dynein heavy chain	35
P-ATPase transporter family	33
Serine peptidase (clan SB, family S8)	33
Membrane trafficking: vesicle fusion	31

protists whose mitochondrial proteomes are reduced (e.g., *Plasmodium*). Because nuclear-encoded hydrogenosomal matrix proteins are targeted to the organelle by N-terminal presequences that are proteolytically cleaved upon import (32) similar to mitochondrial precursor proteins, we screened the genome for consensus 5- to 20-residue presequences containing ML(S/T/A)X_(1...15)R (N/F/E/XF), MSLX_(1...15)R(N/F/XF), or MLR(S/N)F (28) motifs. A total of 138 genes containing putative presequences were identified, 67% of which are similar to known proteins, primarily ones involved in energy metabolism and electron-transport pathways (fig. S13 and table S21).

The production of molecular hydrogen, the hallmark of the hydrogenosome, is catalyzed by an unusually diverse group of iron-only [Fe]-hydrogenases that possess, in addition to a conserved H cluster, four different sets of functional domains (fig. S14), indicating that hydrogen production may be more complex than originally proposed. The pathway that generates electrons for hydrogen (fig. S12) is composed of many proteins encoded by multiple genes (tables S22 to S24). Our analyses extend the evidence that *T. vaginalis* hydrogenosomes contain the complete machinery required for mitochondria-like intraorganellar FeS cluster formation (33) and also reveal the presence of two putative cytosolic auxiliary proteins, indicating that hydrogenosomes may be involved in biogenesis of cytosolic FeS proteins. Some components of

Fig. 3. Structural organization of putative *T. vaginalis* surface molecules involved in host cell adherence and cytotoxicity (28). Candidate surface protein families (a to f) are depicted as part of the glycocalyx (gray shading), known to be composed of LPG (g). The number of proteins with an inferred transmembrane domain (red box) is indicated at right, with the size of the entire family shown in parentheses. Substantial length variation exists between and within families (proteins are not drawn to scale). Additional information can be found in table S18.



FeS cluster assembly machinery have also been found in mitochondria (mitochondrial remnants) of *G. lamblia*, supporting a common evolutionary origin of mitochondria, hydrogenosomes, and mitochondria (3).

A new predicted function of hydrogenosomes revealed by the genome sequence is amino acid metabolism. We identified two components of the glycine-cleavage complex (GCV), L protein and H protein. Another component of this pathway is serine hydroxymethyl transferase (SHMT), which in eukaryotes exists as both cytosolic and mitochondrial isoforms. A single gene coding for SHMT of the mitochondrial type with a putative N-terminal hydrogenosomal presequence was identified. Because both GCV and SHMT require folate (fig. S12), which *T. vaginalis* apparently lacks, the functionality of these proteins remains unclear.

The 5-nitroimidazole drugs metronidazole (Mz) and tinidazole are the only approved drugs for treatment of trichomoniasis. These prodrugs are converted within the hydrogenosome to toxic nitroradicals via reduction by ferredoxin (Fdx) (fig. S12). Clinical resistance to Mz (Mz^R) is estimated at 2.5 to 5% of reported cases and rising (34) and is associated with decreases in or loss of Fdx (35). We identified seven Fdx genes with hydrogenosomal targeting signals (tables S21 and S25), the redundancy of which provides explanations for the low frequency of Mz^R and for why knockout of a single Fdx gene does not lead to Mz^R (35). Our analyses also provide clues to the potential mechanisms that clinically resistant parasites may use, such as the presence of nitroreductase (*NimA*-like), reduced nicotinamide adenine dinucleotide phosphate (NADPH)–

nitroreductase, and NADH-flavin oxidoreductase genes (tables S23 and S26), which have been implicated in Mz^R in bacteria (36, 37).

Summary and concluding remarks. Our investigation of the *T. vaginalis* genome sequence provides a new perspective for studying the biology of an organism that continues to be ignored as a public health issue despite the high number of trichomoniasis cases worldwide. The discovery of previously unknown metabolic pathways, the elucidation of pathogenic mechanisms, and the identification of candidate surface proteins likely involved in facilitating invasion of human mucosal surfaces provide potential leads for the development of new therapies and novel methods for diagnosis.

The analysis presented here of one of the most repetitive genomes known has undoubtedly been hampered by the sheer number of highly similar repeats and transposable elements. Why did this genome expand so dramatically in size? We hypothesize that the most recent common ancestor of *T. vaginalis* underwent a population bottleneck during its transition from an enteric environment (the habitat of most trichomonads) to the urogenital tract. During this time, the decreased effectiveness of selection resulted in repeat accumulation and differential gene family expansion. Genome size and cell volume are positively correlated (38, 39); hence, the increased genome size of *T. vaginalis* achieved through rapid fixation of repeat copies could have ultimately resulted in a larger cell size. *T. vaginalis* cell volume is greater than that of *T. tenax* and related intestinal species *Pentratrichomonas hominis* (40) and *T. gallinae* (41), and it generally conforms to the relationship of genome size to

cell volume reported for protists (41). *T. vaginalis* is also a highly predatory parasite that phagocytoses bacteria, vaginal epithelial cells, and host erythrocytes (42) and is itself ingested by macrophages. Given these interactions, it is tempting to speculate that an increase in cell size could have been selected for in order to augment the parasite's phagocytosis of bacteria, to reduce its own phagocytosis by host cells, and to increase the surface area for colonization of vaginal mucosa.

References and Notes

1. Global Prevalence and Incidence of Selected Curable Sexually Transmitted Infections (World Health Organization, Geneva, 2001), www.who.int/docstore/hiv/GRSTI/006.htm.
2. S. M. Adl et al., *J. Eukaryot. Microbiol.* **52**, 399 (2005).
3. T. M. Embley, W. Martin, *Nature* **440**, 623 (2006).
4. Materials and methods are available as supporting material on Science Online.
5. S. Vanacova, W. Yan, J. M. Carlton, P. J. Johnson, *Proc. Natl. Acad. Sci. U.S.A.* **102**, 4430 (2005).
6. M. A. Schumacher, A. O. Lau, P. J. Johnson, *Cell* **115**, 413 (2003).
7. M. Muller, in *Evolutionary Relationship Among Protozoa*, G. H. Coombs, V. Vickerman, M. A. Sleight, A. Warren, Eds. (Chapman & Hall, London, 1998), pp. 109–132.
8. J. C. Silva, F. Bastida, S. L. Bidwell, P. J. Johnson, J. M. Carlton, *Mol. Biol. Evol.* **22**, 126 (2005).
9. K. Kutisova et al., *Parasitology* **131**, 309 (2005).
10. X. Zuo, B. C. Lockwood, G. H. Coombs, *Microbiology* **141**, 2637 (1995).
11. Y. Kleydman, N. Yarlett, T. E. Gorrell, *Microbiology* **150**, 1139 (2004).
12. P. N. Lowe, A. F. Rowe, *Mol. Biochem. Parasitol.* **21**, 65 (1986).
13. A. C. Turner, W. B. Lushbaugh, *Exp. Parasitol.* **67**, 47 (1988).
14. G. D. Westrop, G. Goodall, J. C. Mottram, G. H. Coombs, *J. Biol. Chem.* **281**, 25062 (2006).
15. D. H. Beach, G. G. Holz Jr., B. N. Singh, D. G. Lindmark, *Mol. Biochem. Parasitol.* **44**, 97 (1991).
16. B. N. Singh, D. H. Beach, D. G. Lindmark, C. E. Costello, *Arch. Biochem. Biophys.* **309**, 273 (1994).
17. C. Vogel, C. Chothia, *PLoS Comput. Biol.* **2**, e48 (2006).
18. M. Parsons, E. A. Worthey, P. N. Ward, J. C. Mottram, *BMC Genomics* **6**, 127 (2005).
19. M. Benchimol, *Microsc. Microanal.* **10**, 528 (2004).
20. T. A. Richards, T. Cavalier-Smith, *Nature* **436**, 1113 (2005).
21. M. A. Ramesh, S. B. Malik, J. M. Logsdon Jr., *Curr. Biol.* **15**, 185 (2005).
22. F. D. Bastida-Corcuera, C. Y. Okumura, A. Colocoussi, P. J. Johnson, *Eukaryot. Cell* **4**, 1951 (2005).
23. B. P. Dias Filho, A. F. Andrade, W. de Souza, M. J. Esteves, J. Angluster, *Microbios* **71**, 55 (1992).
24. A. Ikegami, K. Honma, A. Sharma, H. K. Kuramitsu, *Infect. Immun.* **72**, 4619 (2004).
25. B. Loftus et al., *Nature* **433**, 865 (2005).
26. P. H. Davis et al., *Mol. Biochem. Parasitol.* **145**, 111 (2006).
27. C. Yao, J. E. Donelson, M. E. Wilson, *Mol. Biochem. Parasitol.* **132**, 1 (2003).
28. Single-letter abbreviations for the amino acid residues are as follows: A, Ala; C, Cys; D, Asp; E, Glu; F, Phe; G, Gly; H, His; I, Ile; K, Lys; L, Leu; M, Met; N, Asn; P, Pro; Q, Gln; R, Arg; S, Ser; T, Thr; V, Val; W, Trp; X, any amino acid; and Y, Tyr.
29. M. W. Lehker, T. H. Chang, D. C. Dailey, J. F. Alderete *J. Exp. Med.* **171**, 2165 (1990).
30. P. L. Fiori, P. Rappelli, A. M. Rocchigiani, P. Cappuccinelli, *FEMS Microbiol. Lett.* **109**, 13 (1993).
31. M. Klemba, D. E. Goldberg, *Annu. Rev. Biochem.* **71**, 275 (2002).
32. P. J. Bradley, C. J. Lahti, E. Plumper, P. J. Johnson, *EMBO J.* **16**, 3484 (1997).
33. R. Sutak et al., *Proc. Natl. Acad. Sci. U.S.A.* **101**, 10368 (2004).

34. G. Schmid *et al.*, *J. Reprod. Med.* **46**, 545 (2001).
 35. K. M. Land *et al.*, *Mol. Microbiol.* **51**, 115 (2004).
 36. D. H. Kwon *et al.*, *Antimicrob. Agents Chemother.* **45**, 2609 (2001).
 37. H. K. Leiros *et al.*, *J. Biol. Chem.* **279**, 55840 (2004).
 38. T. Cavalier-Smith, *Ann. Bot. (London)* **95**, 147 (2005).
 39. T. R. Gregory, *Biol. Rev. Camb. Philos. Soc.* **76**, 65 (2001).
 40. B. M. Honigberg, G. Brugerolle, in *Trichomonads Parasitic in Humans*, B. M. Honigberg, Ed. (Springer-Verlag, New York, 1990), pp. 5–35.
 41. B. J. Shuter, *Am. Nat.* **122**, 26 (1983).
 42. J. G. Rendon-Maldonado, M. Espinosa-Cantellano, A. Gonzalez-Robles, A. Martinez-Palomo, *Exp. Parasitol.* **89**, 241 (1998).

43. We are grateful to the *Trichomonas* research community and M. Gottlieb for support and guidance during the duration of this project. We thank M. Delgadillo-Correa, J. Shetty, S. van Aken, and S. Smith for technical support; T. Creasy, S. Angiuoli, H. Koo, J. Miller, J. Orvis, P. Amedeo, and E. Lee for engineering support; W. Majoros and G. Perteu for data manipulation; and S. Sullivan and E. F. Merino for editing. Funding for this project was provided by the National Institute of Allergy and Infectious Diseases (grants U01 AI50913-01 and NIH-N01-AI-30071). The Burroughs Wellcome Fund and the Ellison Medical Foundation provided funds for *Trichomonas* community meetings during the genome project. The Chang Gung *T. vaginalis* Systems Biology Project was supported by grants (SMRPD33002 and SMRPG33115) from Chang Gung Memorial Hospital and Taiwan Biotech Company Limited. This whole genome

shotgun project has been deposited at DNA Data Bank of Japan/European Molecular Biology Laboratory/GenBank under the project accession AAHC00000000. The version described here is the first version, AAHC01000000.

Supporting Online Material

www.sciencemag.org/cgi/content/full/315/5809/207/DC1

Materials and Methods

SOM Text

Figs. S1 to S14

Tables S1 to S26

References

Data

24 July 2006; accepted 14 November 2006

10.1126/science.1132894

REPORTS

Spectropolarimetric Diagnostics of Thermonuclear Supernova Explosions

Lifan Wang,^{1,2*} Dietrich Baade,³ Ferdinando Patat³

Even at extragalactic distances, the shape of supernova ejecta can be effectively diagnosed by spectropolarimetry. We present results for 17 type Ia supernovae that allow a statistical study of the correlation among the geometric structures and other observable parameters of type Ia supernovae. These observations suggest that type Ia supernova ejecta typically consist of a smooth, central, iron-rich core and an outer layer with chemical asymmetries. The degree of this peripheral asphericity is correlated with the light-curve decline rate of type Ia supernovae. These results lend strong support to delayed-detonation models of type Ia supernovae.

Different supernova (SN) explosion mechanisms may lead to differently structured ejecta. Type Ia supernovae (SNe) have been used as premier tools for precision cosmology. They occur when a carbon and oxygen white dwarf reaches the Chandrasekhar stability limit, probably because of mass accretion in a binary system, and is disrupted in a thermonuclear explosion (1). Decade-long debates have discussed how the explosive nuclear burning is triggered and how it propagates through the progenitor star (2–6). Successful models generally start with a phase of subsonic nuclear burning, or deflagration, but theorists disagree on whether the burning front becomes supersonic after the earlier phase of deflagration. An explosion that does turn into supersonic burning is called delayed detonation (4). The resulting chemical structures are dramatically different for deflagration (5) and delayed-detonation models (7). For a pure deflagration model, chemical clumps are expected to be present at all velocity layers that burning has reached (5). For delayed detonation, the detonation front propagates

through the ashes left behind by deflagration, burns partially burned or unburned elements further into heavier elements, and erases the chemically clumpy structures generated by deflagration.

The polarized emission from a supernova is caused by electron scattering in its ejecta. It is

sensitive to the geometric structure of the ejecta (8). Electron scattering in an asymmetric ejecta would produce nonzero degrees of polarization (8). In continuum light, normal SNe Ia are only polarized up to about 0.3%, but polarization as high as 2% is found across some spectral lines (9–14). The polarization decreases with time and vanishes around 2 weeks past optical maximum. The low level of continuum polarization implies that the SN Ia photospheres are, in general, almost spherical. The decrease of polarization at later times suggests that the outermost zones of the ejecta are more aspherical than the inner zones. Similarly, the large polarization across certain spectral lines implies that the layers above the photosphere are highly aspheric and most likely chemically clumpy (12–15).

In this study, we report polarimetry of 17 SNe Ia. These are all the SNe Ia for which we have premaximum polarimetry. The observations (Table 1) were collected with the 2.1-m Otto Struve Telescope of the McDonald Observatory of the University of Texas and with one of the 8.2-m

Table 1. Identification, observing date, phase (in days relative to optical maximum light), telescope (McD indicates McDonald Observatory), intrinsic degree of polarization across the Si II 635.5-nm line, Δm_{15} , and references for Δm_{15} values. Numbers in parentheses indicate 1- σ error multiplied by 100.

SN	Date of observation	Phase	Telescope	P_{SiII}	Δm_{15}	References
1996X	14 April 1996	−4.2	McD 2.1 m	0.50(20)	1.30(02)	(19, 21)
1997bp	7 April 1997	−5.0	McD 2.7 m	0.90(10)	1.29(08)	(19, 22)
1997bq	25 April 1997	−3.0	McD 2.1 m	0.40(20)	1.17(02)	(19, 22)
1997br	20 April 1997	−2.0	McD 2.1 m	0.20(20)	1.09(02)	(19, 23)
1999by	9 May 1999	−2.5	McD 2.1 m	0.40(10)	1.79(01)	(24)
2001V	25 February 2001	−7.3	VLT	0.00(07)	0.73(03)	(19, 25)
2001el	26 September 2001	−4.2	VLT	0.45(02)	1.16(01)	(19, 26)
2002bo	18 March 2002	−5.0	VLT	0.90(05)	1.34(03)	(19, 27)
2002el	14 August 2002	−6.4	VLT	0.72(09)	1.38(05)	(19)
2002fk	6 October 2002	−5.5	VLT	0.67(10)	1.19(05)	see text
2003W	31 January 2003	−4.5	VLT	0.64(10)	1.30(05)	see text
2004dt	13 August 2004	−7.3	VLT	1.60(10)	1.21(05)	(28)
2004ef	11 September 2004	−4.1	VLT	1.10(30)	1.54(07)	see text
2004eo	20 September 2004	−5.9	VLT	0.71(08)	1.46(08)	(28)
2005cf	1 June 2005	−9.9	VLT	0.44(05)	1.12(06)	(28)
2005de	6 August 2005	−4.4	VLT	0.67(14)	1.41(06)	see text
2005df	8 August 2005	−4.3	VLT	0.73(05)	1.29(09)	see text

¹Physics Department, Texas A&M University, College Station, TX 77843–4242, USA. ²Lawrence Berkeley National Laboratory, Berkeley, CA 94720, USA. ³European Southern Observatory, Karl-Schwarzschild-Strasse 2, D-85748 Garching, Germany.

*To whom correspondence should be addressed. E-mail: wang@physics.tamu.edu